SUPPLEMENTAL FIGURES

This file contains Figure S1-S7, including Supplemental Figure Legends.

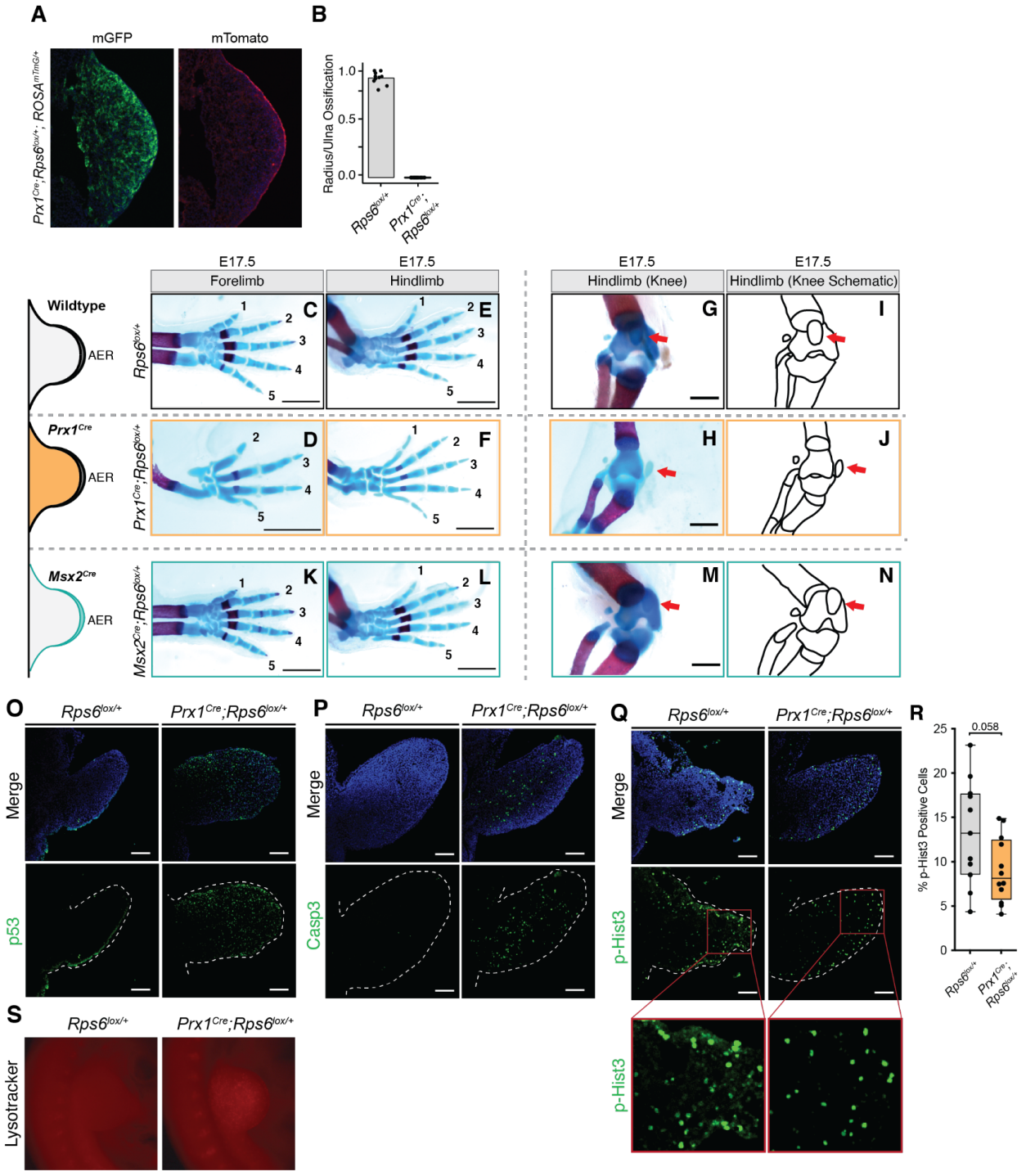

Figure S1. *Rps6* haploinsufficiency leads to patterning defects and non-spatially restricted p53 activation. Related to Figure 1.

(**A**) Representative tissue section from E9.5 *Prx1^{Cre};Rps6$^{lox/+}$;Rosa$^{mTmG/+}$* forelimb bud demonstrating distribution of recombination in the developing limb bud. green = recombined membrane GFP; red = unrecombined membrane Tomato.
(**B**) Degree and penetrance of radial aplasia was measured by quantifying the ratio of the length of radius ossification compared to that of the ulna in E17.5 forelimbs. *n* = 10 limbs (*Rps6$^{lox/+}$*), *n* = 28 limbs (*Prx1^{Cre};Rps6$^{lox/+}$*). Quantification demonstrates significant and penetrant radial aplasia in *Prx1^{Cre};Rps6$^{lox/+}$* embryos compared to control.
(**C-N**) Characterization of phenotypes associated with *Rps6* haploinsufficiency. **Left**: Digit phenotypes found in the forelimb and hindlimb of WT *Rps6$^{lox/+}$* (top row), *Prx1^{Cre};Rps6$^{lox/+}$* (middle row), and *Msx2^{Cre};Rps6$^{lox/+}$* (bottom row) E17.5 embryos, Numbers label digits. **Right**: Patella phenotypes found in the hindlimb of WT *Rps6$^{lox/+}$* (top row), *Prx1^{Cre};Rps6$^{lox/+}$* (middle row), and *Msx2^{Cre};Rps6$^{lox/+}$* (bottom row) E17.5 embryos. Red arrows denote the patella.
(**O-Q**) Tissue sections from E10.5 WT (*Rps6$^{lox/+}$*) and *Prx1^{Cre};Rps6$^{lox/+}$* forelimbs stained (green) for p53 (**O**); cleaved Caspase-3, a marker of apoptosis (**P**); and phospho-Histone H3 (p-Hist3), a marker of cell proliferation (**Q**). DAPI staining shown in blue.
(**R**) Percentage of phospho-Histone H3-labeled cells from tissue sections of E10.5 WT (*Rps6$^{lox/+}$*) and *Prx1^{Cre};Rps6$^{lox/+}$* forelimbs. *n* = 11 sections from 3 embryos (WT); *n* = 12 sections from 3 embryos (*Prx1^{Cre};Rps6$^{lox/+}$*).
(**S**) Whole mount Lysotracker Red staining for E10.5 forelimbs from WT (*Rps6$^{lox/+}$*) and *Prx1^{Cre};Rps6$^{lox/+}$* embryos as a marker of cell death.

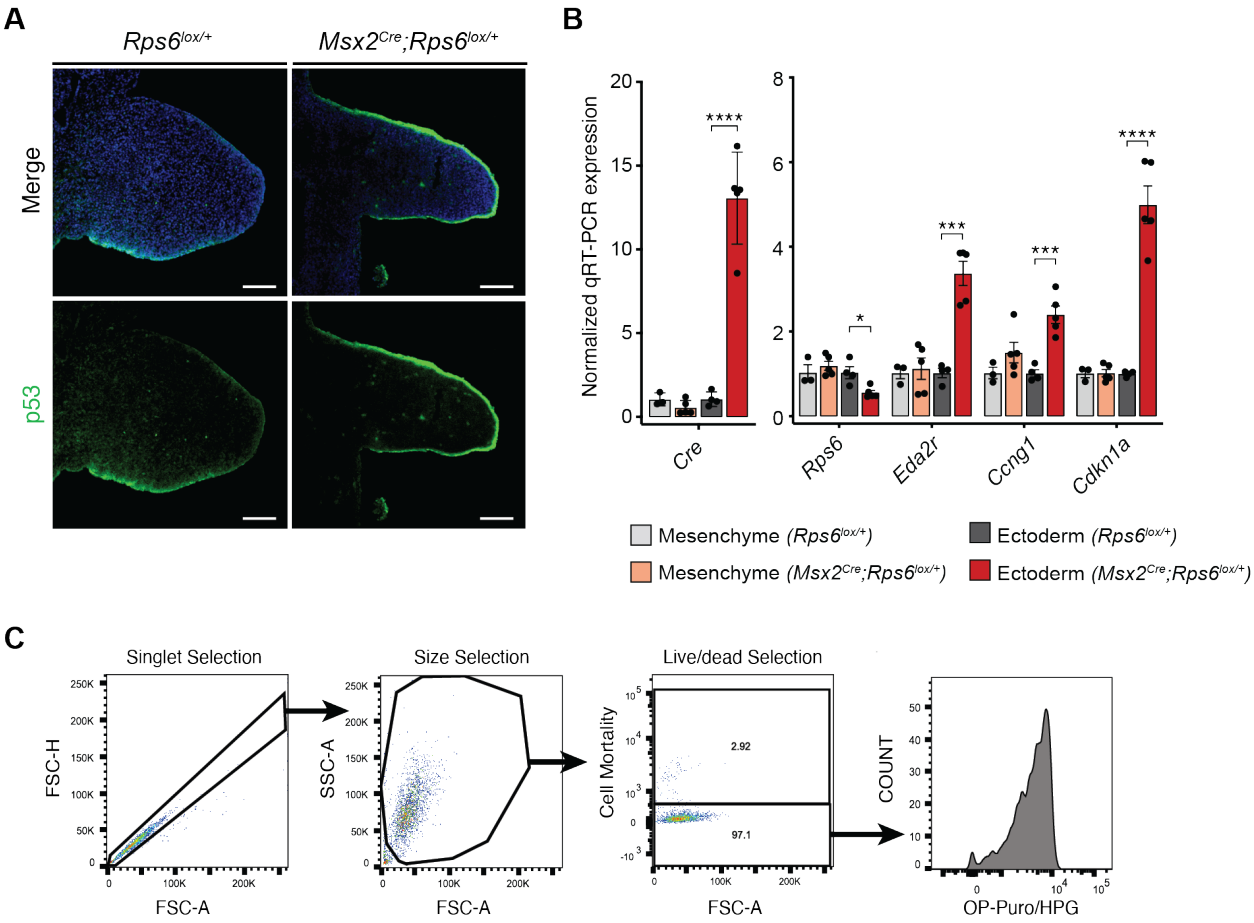

Figure S2. p53 is active in the AER of *Msx2^{cre};Rps6$^{lox/+}$* limbs, and overview of flow cytometry gating schemes for OPP and HPG labeling experiments. Related to Figure 1.

(**A**) Tissue sections from E10.5 WT (*Rps6$^{lox/+}$*) and *Msx2^{Cre};Rps6$^{lox/+}$* forelimbs stained for p53 (green) and DAPI (blue).

(**B**) RT-qPCR of select p53 target genes and *Rps6* mRNA from isolated ectoderm or mesenchyme layers from E11.5 WT (*Rps6$^{lox/+}$*) and *Msx2^{Cre};Rps6$^{lox/+}$* forelimbs. Expression was normalized to *Actb* and *NupL1* as housekeeping genes and then to the mean of WT for each tissue. Error bars = SEM, * $P < 0.05$, ** $P < 0.01$, *** $P < 0.001$, **** $P < 0.0001$, two-tailed t-test, unequal variance.

(**C**) Gating scheme for OPP and HPG incorporation assays. FACS gates of analyzed cells labeled with Zombie Violet Live-Dead Stain and Alexa Fluor 555 Picolyl Azide dye after incorporation of OPP or HPG.

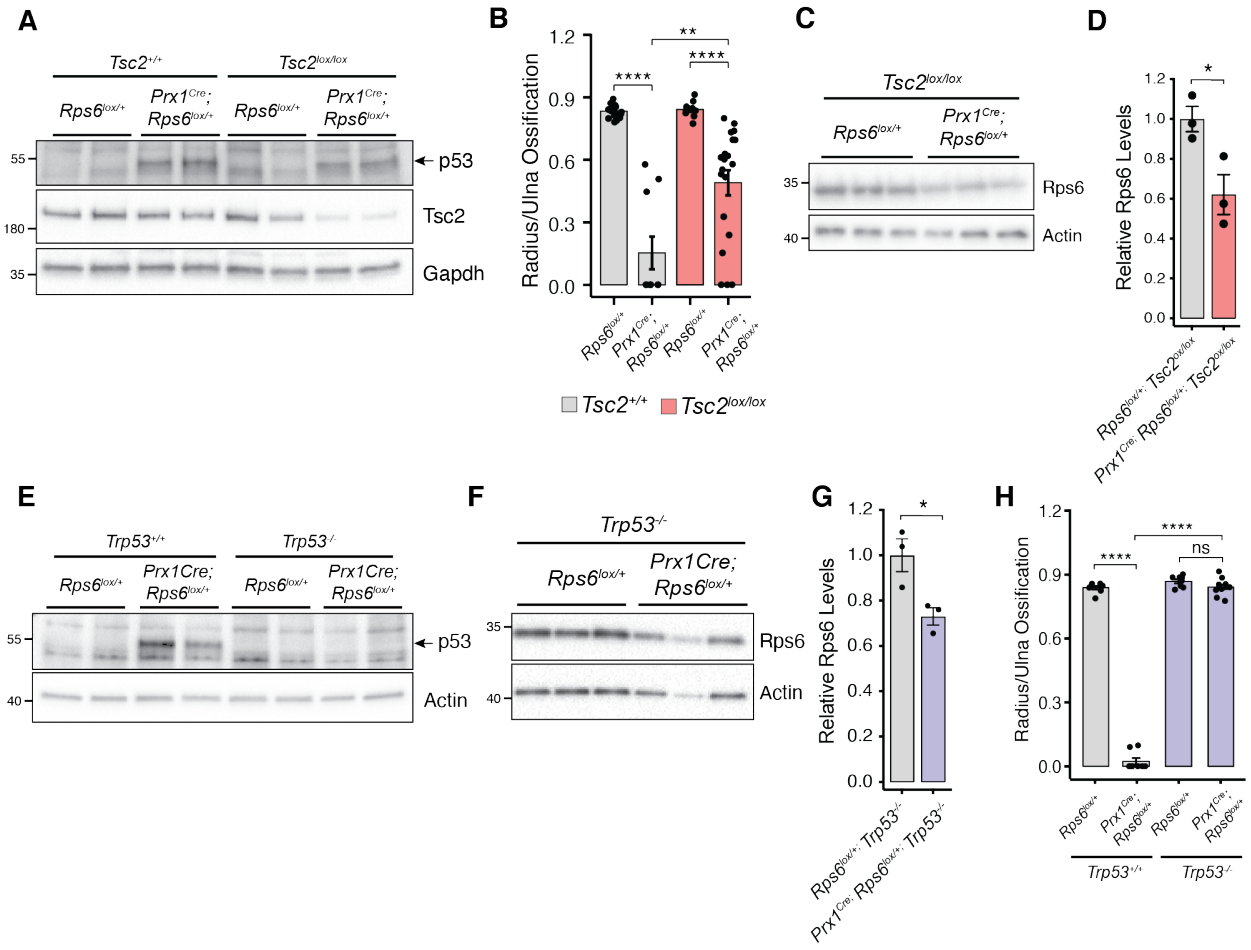

Figure S3. Both loss of *Tsc2* and p53 deletion rescue limb phenotype and protein synthesis upon *Rps6* haploinsufficiency. Related to Figure 2.

(**A**) Western blot of p53 and Tsc2 from whole E10.5 forelimbs of *Rps6*$^{lox/+}$;*Tsc2*$^{+/+}$, *Prx1*^{Cre};*Rps6*$^{lox/+}$;*Tsc2*$^{+/+}$, *Rps6*$^{lox/+}$;*Tsc2*$^{lox/lox}$, and *Prx1*^{Cre};*Rps6*$^{lox/+}$;*Tsc2*$^{lox/lox}$ embryos showing that p53 is still activated upon *Rps6* haploinsufficiency in a *Tsc2* conditional null background.

(**B**) Quantification of radius/ulna ossification length in E17.5 forelimbs. *n* = 18 limbs, (*Rps6*$^{lox/+}$;*Tsc2*$^{+/+}$); *n* = 10 limbs, (*Prx1*^{Cre};*Rps6*$^{lox/+}$;*Tsc2*$^{+/+}$); *n* = 10 limbs, (*Rps6*$^{lox/+}$;*Tsc2*$^{lox/lox}$); *n* = 20 limbs, (*Prx1*^{Cre};*Rps6*$^{lox/+}$;*Tsc2*$^{lox/lox}$).

(**C**) Western blot of Rps6 from whole E10.5 forelimbs of *Rps6*$^{lox/+}$;*Tsc2*$^{lox/lox}$ and *Prx1*^{Cre};*Rps6*$^{lox/+}$;*Tsc2*$^{lox/lox}$ embryos showing that Rps6 is still decreased upon *Rps6* haploinsufficiency in a *Tsc2* conditional null background.

(**D**) Quantification of Rps6 levels in (C) normalized to Actin and to WT embryos.

(**E**) Western blot of p53 from whole E10.5 forelimbs from *Rps6*$^{lox/+}$;*Trp53*$^{+/+}$, *Prx1*^{Cre};*Rps6*$^{lox/+}$;*Trp53*$^{+/+}$, *Rps6*$^{lox/+}$;*Trp53*$^{-/-}$, and *Prx1*^{Cre};*Rps6*$^{lox/+}$;*Trp53*$^{-/-}$ embryos.

(**F**) Representative Western blot of Rps6 from whole *Rps6*$^{lox/+}$;*Trp53*$^{-/-}$, and *Prx1*^{Cre};*Rps6*$^{lox/+}$;*Trp53*$^{-/-}$ forelimbs at E10.5 showing that Rps6 is still decreased upon *Rps6* haploinsufficiency in a *Trp53* null background.

(**G**) Quantification of Rps6 levels in (F) normalized to Actin and to WT embryos.
(**H**) Quantification of radius/ulna ossification in E17.5 forelimbs. n = 8 limbs, (*Rps6*$^{lox/+}$*;Trp53*$^{+/+}$); n = 8 limbs, (*Prx1*^{Cre}*;Rps6*$^{lox/+}$*;Trp53*$^{+/+}$); n = 8 limbs, (*Rps6*$^{lox/+}$*;Trp53*$^{-/-}$); n = 12 limbs, (*Prx1*^{Cre}*;Rps6*$^{lox/+}$*;Trp53*$^{-/-}$). Error bars = SEM, * $P < 0.05$, ** $P < 0.01$, *** $P < 0.001$, **** $P < 0.0001$, two-tailed t-test, unequal variance.

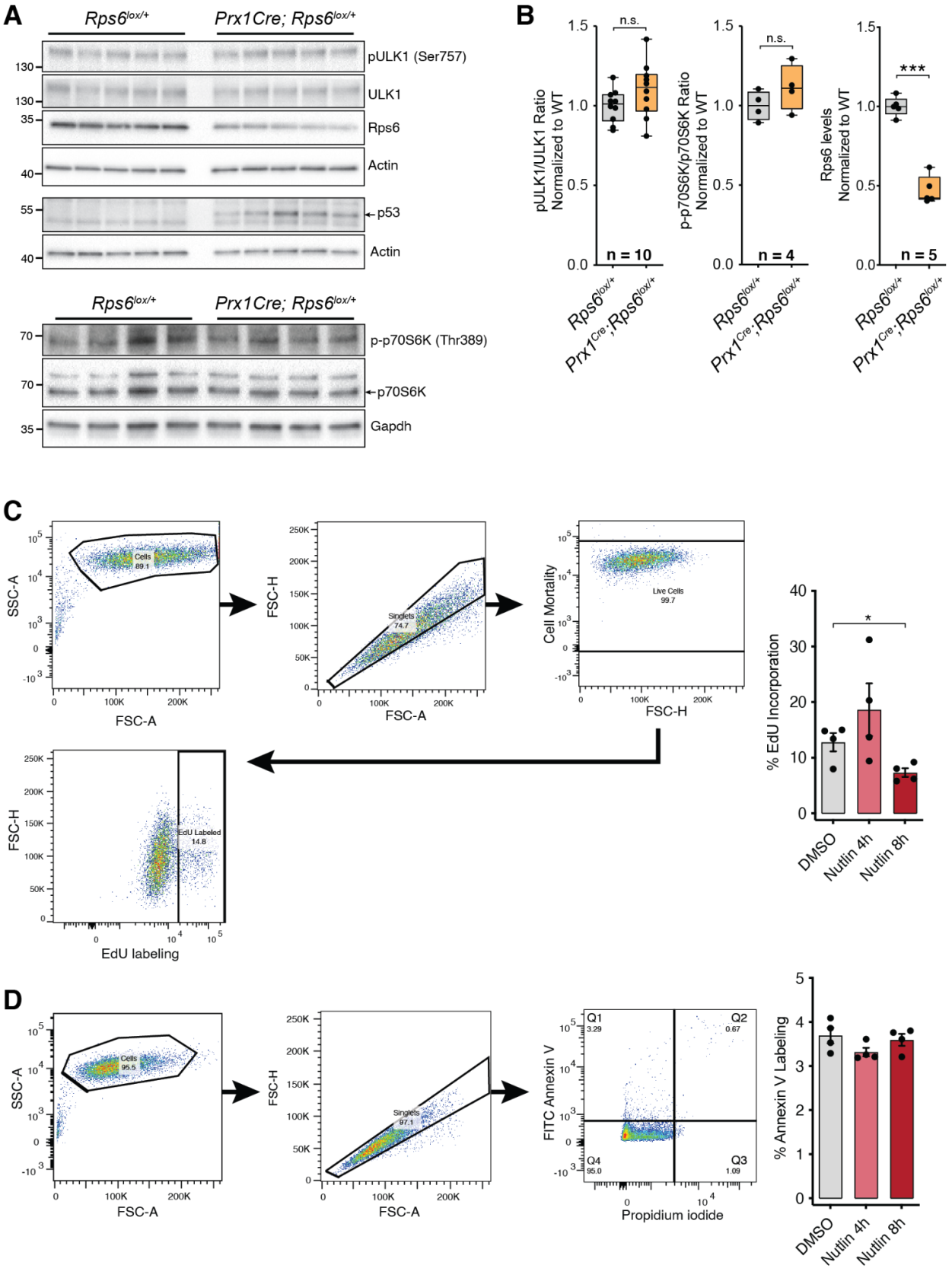
A
Rps6lox/+
Prx1Cre; Rps6lox/+
130
pULK1 (Ser757)
130
ULK1
35
Rps6
40
Actin
55
p53
40
Actin
Rps6lox/+
Prx1Cre; Rps6lox/+
70
p-p70S6K (Thr389)
70
p70S6K
35
Gapdh
B
pULK1/ULK1 Ratio Normalized to WT
n.s.
n = 10
p-p70S6K/p70S6K Ratio Normalized to WT
n.s.
n = 4
Rps6 levels Normalized to WT
***
n = 5
Rps6lox/+
Prx1Cre;Rps6lox/+
C
SSC-A
FSC-A
Cells
89.1
FSC-H
Singlets
74.7
Cell Mortality
Live Cells
99.7
EdU labeling
EdU Labeled
14.8
% EdU Incorporation
DMSO
Nutlin 4h
Nutlin 8h
D
SSC-A
FSC-A
Cells
95.5
FSC-H
Singlets
97.1
FITC Annexin V
Propidium iodide
Q1
3.29
Q2
0.67
Q4
95.0
Q3
1.09
% Annexin V Labeling
DMSO
Nutlin 4h
Nutlin 8h

Figure S4. *Rps6* haploinsufficiency demonstrates an increase in p53 protein, a decrease in Rps6, and no significant perturbation of mTORC1 pathway activity; and Nutlin-3a treatment causes translational repression with minimal effects on cell proliferation and apoptosis. Related to Figures 1-3.

(**A**) Representative Western blots of p53, Rps6, and phosphorylated proteins targeted by the mTORC1 pathway (ULK1, p70S6K). Each lane represents whole forelimbs from an individual *Rps6*$^{lox/+}$ or *Prx1*^{Cre}*;Rps6*$^{lox/+}$ E10.5 embryo.

(**B**) Quantification of Western blots for Rps6 in addition to mTOR pathway targets. For mTOR pathway targets, each protein was normalized to its non-phosphorylated form and then to WT (*Rps6*$^{lox/+}$). For phospho-ULK1, quantification was done for 10 limbs over two blots. Rps6 quantification was normalized to Actin and WT *Rps6*$^{lox/+}$.

(**C**) FACS gating scheme of NIH3T3 fibroblast cells labeled with Zombie Violet Live-Dead Stain and Alexa Fluor 488 Azide dye after incorporation of EdU to measure cell proliferation. Right: percentage of EdU-positive cells after treatment with DMSO or Nutlin-3a for 4 and 8 h.

(**D**) FACS gating scheme of NIH3T3 fibroblast cells stained with Annexin V and propidium iodide to measure levels of apoptosis. Right: percentage of Annexin V-labeled cells in Q1 after treatment with DMSO or Nutlin-3a for 4 and 8 h.

For all blots equal amounts of limb lysate was used for detection.

For box-plots, center line, median; box limits, first and third quartiles; whiskers, max or min value no further than 1.5x interquartile range. * $P < 0.05$, two-tailed t-test, unequal variance.

For bar plots, error bars = SEM, * $P < 0.05$, ** $P < 0.01$, *** $P < 0.001$, **** $P < 0.0001$, two-tailed t-test, unequal variance.

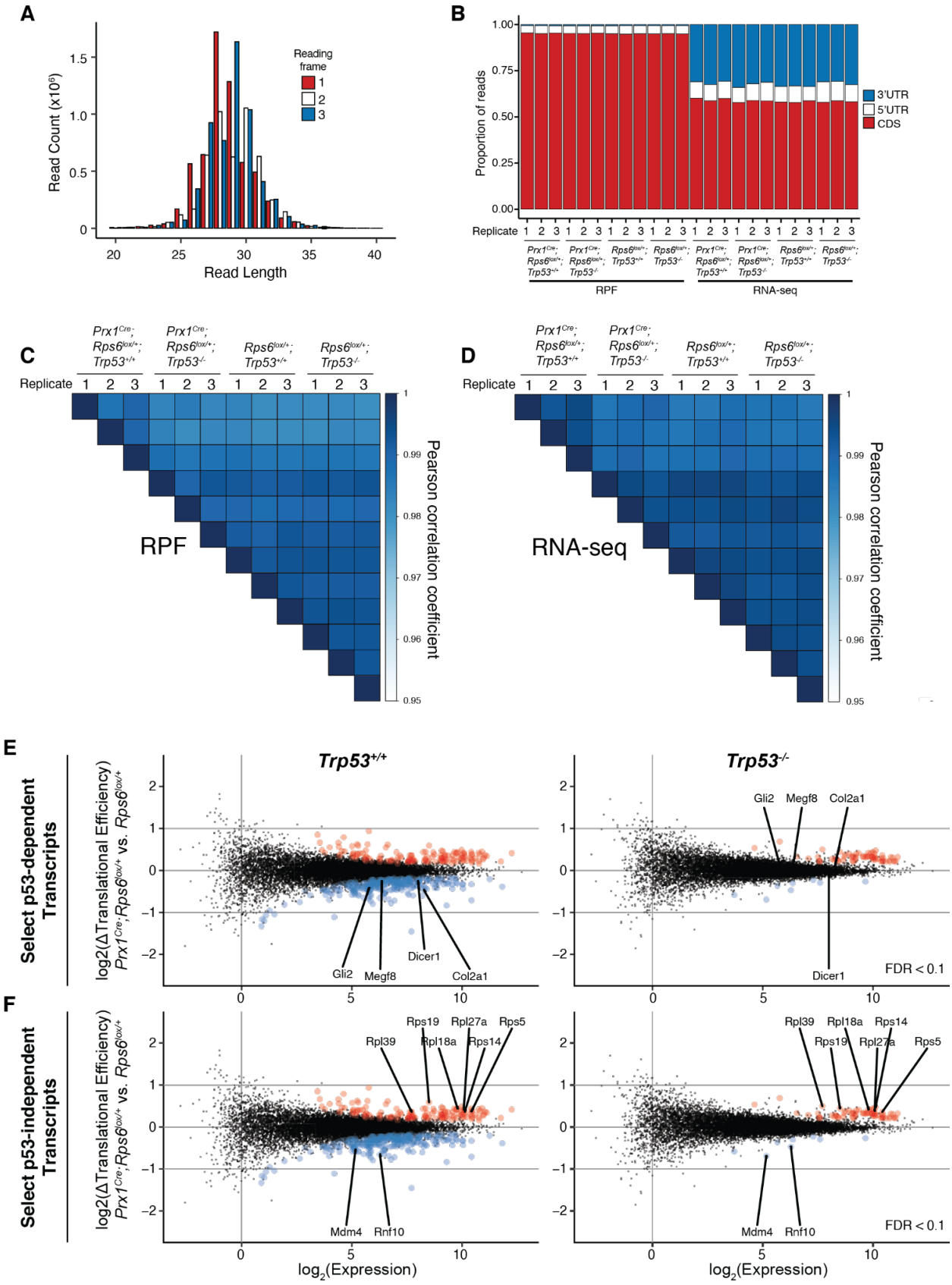
A
Read Count (x10^6)
Read Length
Reading frame
1
2
3
B
Proportion of reads
3'UTR
5'UTR
CDS
Replicate
RPF
RNA-seq
C
RPF
Pearson correlation coefficient
D
RNA-seq
Pearson correlation coefficient
E
Trp53+/+
Trp53-/-
Select p53-dependent Transcripts
log2(ΔTranslational Efficiency) Prx1Cre;Rps6lox/+ vs. Rps6lox/+
Gli2
Megf8
Dicer1
Col2a1
FDR < 0.1
F
Select p53-independent Transcripts
Rps19
Rpl27a
Rps5
Rpl39
Rpl18a
Rps14
Mdm4
Rnf10
log2(Expression)

Figure S5. Quality control and analysis of ribosome profiling experiments. Related to Figure 4.

(**A**) Read length and CDS reading frame distribution for ribosome protected fragments (RPF) aligning to annotated ORFs in a representative library. Note that RNase A and T1 cut single-stranded RNA at only C/U and G, respectively, thus accounting for the slightly incoherent frame distribution (see Method Details).

(**B**) Proportion of reads aligning to CDS, 5'UTR, and 3'UTR regions from RPF and RNA-Seq libraries. Note the expected CDS enrichment for ribosome protected fragments.

(**C-D**) Correlation matrix displaying sample-to-sample Pearson correlation coefficients for (C) RPF and (D) RNA-Seq $\log_2$(counts per million reads).

(**E-F**) Corresponding MA plots of change in translational efficiency (ΔTE) in whole E10.5 *Prx1*^{Cre}*;Rps6*$^{lox/+}$ vs. *Rps6*$^{lox/+}$ embryonic forelimbs in a *Trp53*$^{+/+}$ or *Trp53*$^{-/-}$ background, highlighting select limb developmental transcripts with p53-dependent changes (**E**) and select transcripts with p53-independent changes (**F**). Note that 50 of the 64 significant translationally upregulated p53-independent transcripts consist of RPs (Table S4). Although standard ribosome profiling cannot detect alterations in global protein synthesis, this technique can pinpoint relative changes in the translation efficiency (TE) of specific transcripts (McGlincy and Ingolia, 2017).

Red, ΔTE > 0; blue, ΔTE < 0; n = 3 biological replicates (2 embryos each); FDR < 0.1.

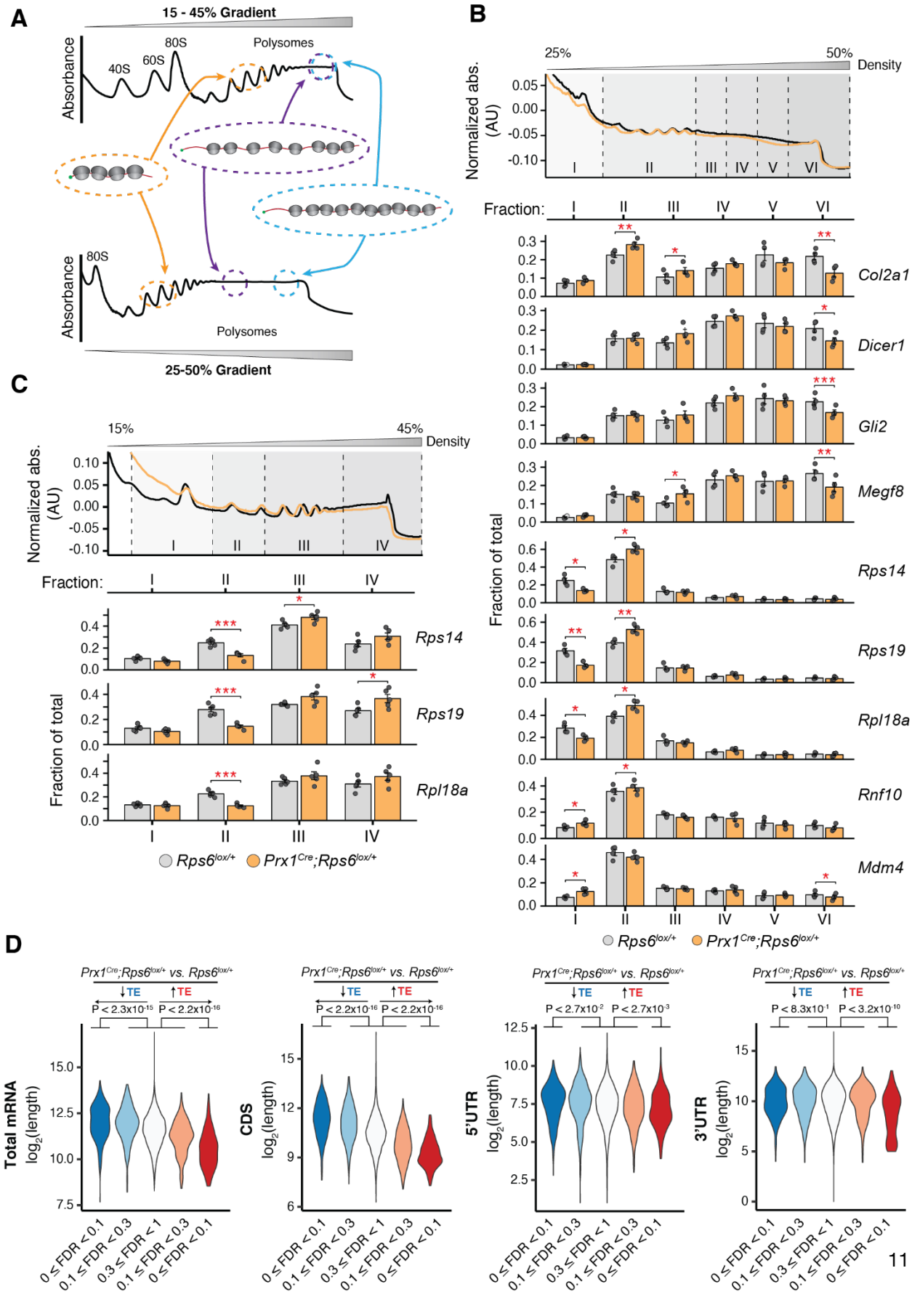
A
15 - 45% Gradient
80S
60S
40S
Polysomes
Absorbance
80S
Polysomes
Absorbance
25-50% Gradient
B
25%
50%
Density
Normalized abs. (AU)
I
II
III
IV
V
VI
Fraction:
Col2a1
Dicer1
Gli2
Megf8
Rps14
Rps19
Rpl18a
Rnf10
Mdm4
Fraction of total
Rps6lox/+
Prx1Cre;Rps6lox/+
C
15%
45%
Density
Normalized abs. (AU)
Fraction:
Rps14
Rps19
Rpl18a
Fraction of total
Rps6lox/+
Prx1Cre;Rps6lox/+
D
Prx1Cre;Rps6lox/+ vs. Rps6lox/+
↓TE
↑TE
P < 2.3x10-15
P < 2.2x10-16
P < 2.2x10-16
P < 2.2x10-16
P < 2.7x10-2
P < 2.7x10-3
P < 8.3x10-1
P < 3.2x10-10
Total mRNA log2(length)
CDS log2(length)
5'UTR log2(length)
3'UTR log2(length)
0 ≤ FDR < 0.1
0.1 ≤ FDR < 0.3
0.3 ≤ FDR < 1
0.1 ≤ FDR < 0.3
0 ≤ FDR < 0.1

Figure S6. Sucrose gradient polysome fractionation and RT-qPCR validation of high-confidence differentially translated ribosome profiling candidate transcripts; and *cis*-RNA features associated with translation changes upon *Rps6* haploinsufficiency. Related to Figure 4.

(**A**) Diagram of mRNAs co-fractionating with polysomes in sucrose density gradients. Note that mRNA transcript and ORF length impact the sensitivity of polysome gradients to resolve shifts in polysome profiles. Transcripts that are shorter in length inherently have less ribosomes bound, and thus appear earlier in the gradient fractions, while longer mRNAs naturally appear in the more dense fractions of the gradient. Less dense gradients, which better separate transcripts bound to relatively few ribosomes, are therefore better at resolving changes in ribosome occupancy for shorter transcripts whereas more dense gradients, which better separate transcripts bound to many ribosomes, are better at resolving changes for longer transcripts. Given the strong length dependency of translationally changing transcripts upon *Rps6* haploinsufficiency (Figure 4E), different density gradients (15-45%, 25-50%) were performed to resolve changes in various length transcripts.

(**B-C**) Ribosome profiling results were validated using sucrose gradient polysome fractionation and subsequent RT-qPCR on select, differentially translated transcripts from E10.5 $Prx1^{Cre};Rps6^{lox/+}$ and $Rps6^{lox/+}$ limb buds. RT-qPCR of select mRNAs from 25-50% (**B**) and 15-45% (**C**) sucrose density gradients from whole E10.5 WT (gray) or $Prx1^{Cre};Rps6^{lox/+}$ (orange) limb buds. RT-qPCR Ct values were normalized to spike-in *in vitro* transcribed Renilla luciferase RNA added to each fraction and then to the sum total of all fractions. Upon *Rps6* haploinsufficiency, we observed a shift to lighter polysomes for transcripts whose TE decreased in the ribosome profiling (e.g., *Col2a1, Dicer1, Gli2, Megf8, Mdm4,* and *Rnf10*) and observed a shift towards heavier polysomes for transcripts whose TE increased in the ribosome profiling (e.g., RPs). **Top**: polysome trace from WT (gray) or $Prx1^{Cre};Rps6^{lox/+}$ (orange) limb buds. **Bottom**: RT-qPCR of select mRNAs. * $P < 0.05$, ** $P < 0.01$, *** $P < 0.001$, two-tailed t-test, paired.

(**D**) Violin plots quantifying ΔTE relative to total mRNA, CDS, 5'UTR, and 3'UTR length. Transcripts are stratified by direction of TE change (blue, down; red, up) and FDR ($0 \leq FDR < 0.1$, $0.1 \leq FDR < 0.3$, $0.3 \leq FDR \leq 1$); Mann-Whitney U test. Transcript length, driven largely by CDS length, is negatively correlated with translation efficiency changes upon *Rps6* haploinsufficiency.

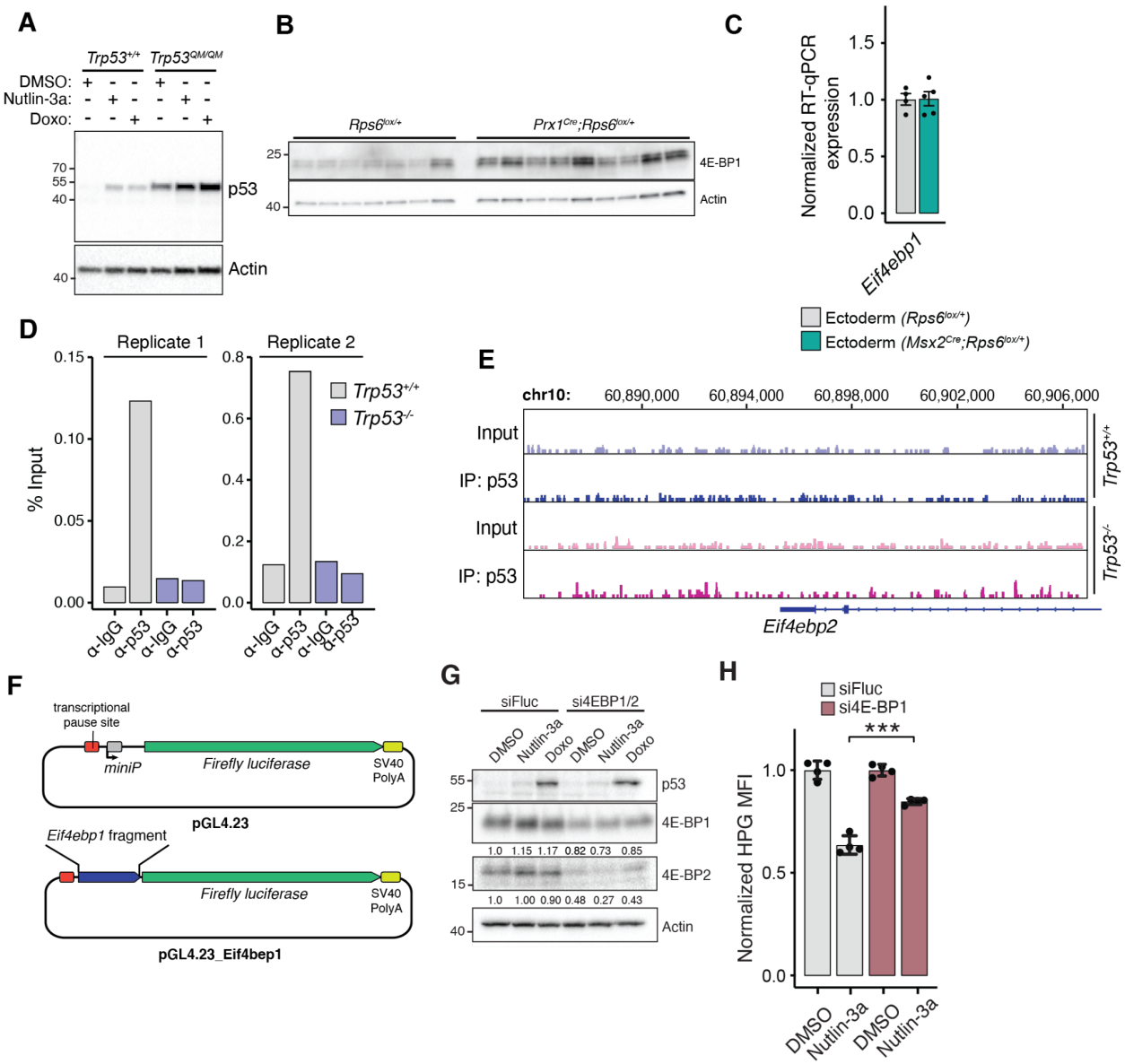

Figure S7. p53 transcriptional activity is required for translational repression; p53 induces *Eif4ebp1* expression; and depletion of 4E-BP1 restores p53-induced translation defects. Related to Figures 5-6.

(**A**) Western blot of p53 stabilization after 8 h of Nutlin-3a or Doxo treatment of MEFs harboring WT (*Trp53*$^{+/+}$) or transactivation dead mutant (*Trp53*$^{QM/QM}$) p53. Of note, the *Trp53*^{QM} allele also abrogates Mdm2 mediated degradation of p53, thus stabilizing p53 at baseline without drug treatment (Kenzelmann Broz et al., 2013).

(**B**) Full Western blot from Figures 5E-F of 4E-BP1 from E10.5 *Rps6*$^{lox/+}$ and *Prx1*^{Cre}*;Rps6*$^{lox/+}$ forelimb mesenchyme cells after removal of the ectoderm layer. The outer unrecombined ectoderm layer was removed to enrich for recombined mesenchyme given the lower sensitivity of immunoblot analysis compared to RT-qPCR.

(**C**) RT-qPCR of *Eif4ebp1* mRNA from ectoderm isolated from E11.5 WT (*Rps6*$^{lox/+}$) and *Msx2*^{Cre};*Rps6*$^{lox/+}$ forelimbs. Expression was normalized to *Actb* and *NupL1* and then to WT.
(**D**) ChIP-qPCR of p53 or IgG control from WT or *Trp53* null MEFs treated with Doxo using gene-specific primers for *Eif4ebp1*. Shown is the percent input of two independent replicates.
(**E**) p53 ChIP-Seq gene track of the *Eif4ebp2* locus (Kenzelmann Broz et al., 2013) from Doxo-treated *Trp53*$^{+/+}$ and *Trp53*$^{-/-}$ MEFs.
(**F**) Schematic of constructs used to test p53-dependent promoter activity at the *Eif4ebp1* locus in Figure 5K.
(**G**) Western blot of 4E-BP1 and 4E-BP2 levels after 16 h of siRNA depletion in NIH3T3 cells. Numbers indicate the amount of quantified protein normalized to Actin and compared to control cells treated with DMSO and control siFluc.
(**H**) Quantification of HPG MFI upon siRNA knockdown of only *Eif4ebp1* and control siFluc in NIH3T3 cells normalized to mean of respective DMSO control for each knockdown condition; $n = 4$.
For all bar plots, error bars = SEM, * $P < 0.05$, ** $P < 0.01$, *** $P < 0.001$, **** $P < 0.0001$, two-tailed t-test, unequal variance.